Design of a Highly Stable, High-Conversion-Efficiency, Optical Parametric Chirped-Pulse Amplification System with Good Beam Quality

Introduction

Optical parametric chirped-pulse amplification (OPCPA) has been shown[1–7] to be well suited for front-end amplification in petawatt-class laser systems. The high-gain and large-gain bandwidth available in type-I parametric amplification using a relatively short length of material affords low spectral phase distortion and low *B*-integral accumulation.[2] Prepulses typical of multipass regenerative amplifiers are eliminated with simple, single-pass OPCPA arrangements, and the low thermal loading in the parametric process reduces undesirable thermal effects. The requirement for 100-mJ-level, 1054-nm chirped pulses operating at a moderate repetition rate (~5 Hz) for front-end injection into a glass-amplifier chain places significant demands on the OPCPA pump laser.[3,5,7] The spatial and temporal characteristics of commercial pump lasers have limited their ability to achieve high pump-to-signal conversion efficiency through the OPCPA process.[6] Recently, we reported a measurement of 29% conversion efficiency in a single-stage OPCPA at a 5-Hz repetition rate, with over 6×10^6 gain, 5-mJ output energy, and output stability better than that of the pump laser.[7] Efficient and stable OPCPA output was achieved by carefully designing the OPCPA configuration and by optimizing the spatiotemporal profile of the pump. This significantly reduced the average power requirement of the pump laser.

The maximum OPCPA conversion efficiency is obtained when the rate of energy transfer from the pump to the signal and idler is such that all spatial and temporal points in the pulse reach peak conversion simultaneously. Maximizing the conversion efficiency thus requires the use of complementary shapes for the seed and pump spatial and temporal profiles, as described by Begishev *et al.*[8,9] Appropriate seed temporal shapes can be approximated by spectral shaping[10] or other pulse-shaping techniques.[11,12] Ross *et al.*[12] described a multiple-stage OPCPA design that allows significant reconversion in the preamplifier stages in order to produce an approximately complementary seed shape for use with a temporally Gaussian shaped pump in the final power-amplifier stage. Since most of the pump-to-signal energy exchange will occur in the power amplifier, a high conversion efficiency may be obtained if the seed and pump spatial shapes are also properly matched. This approach would be particularly attractive if it were desired to achieve a high pulse contrast after recompression in an all-OPCPA system without the gain shaping expected through a glass-amplifier chain.[13] If independent control of the spatial and temporal shapes does not exist, then spatiotemporal coupling in the OPCPA process may limit the ability to simultaneously achieve high efficiency, high stability, high pulse contrast, and good beam quality. It is therefore important to understand the detailed spatiotemporal behavior of the OPCPA process in order to fully optimize a design.

Flattop shapes for both seed and pump can also be used and can be approximated by high-order, super-Gaussian spatial and temporal shapes. Our work has shown that when the spatial and temporal shapes of the pump are high-order super-Gaussians, high conversion efficiency can be attained without the need to explicitly shape the seed pulse.[7] The very high gain provided by the optical parametric amplification process shapes the originally Gaussian spatiotemporal profile of the seed so that the full widths at half maximum (FWHM) of the signal and pump are well matched when the amplification process begins to saturate. In the high-gain region of the amplifier, however, the finite slope of the edges of the pump beam and finite rise and fall times of the pump pulse can limit the amount of pump energy extracted due to gain narrowing.[14] Gain narrowing caused by spatial and temporal variations of the pump intensity limits the overlap area of the pump and signal, reducing the energy extracted from the pump. Although the effect of gain narrowing can be reduced by heavily saturating the amplifier,[14] high-order super-Gaussian shapes are preferred to both reduce the gain narrowing and maximize the conversion efficiency.

Several articles[2,3,12,14] have discussed OPCPA performance for temporal Gaussian shapes and Gaussian or flattop spatial shapes. This article extends this discussion by using a numerical model to systematically investigate the performance

of an OPCPA system using both Gaussian and super-Gaussian spatial and temporal shapes. This investigation includes the effects of pump–signal spatial walk-off and spatiotemporal noise to obtain good energy stability, good beam quality, and high overall conversion efficiency.

In the following sections, (1) the design goals for our OPCPA system are briefly discussed; (2) the numerical model is described; (3) a single-stage OPCPA system with no spatiotemporal noise on the input beams is considered, and it is shown that for OPA crystals with large pump–signal walk-off, such as beta-barium borate (BBO), operation of the system in the region of enhanced stability can degrade the near-field beam shape and slightly reduce efficiency; (4) a comparison is made with lithium triborate (LBO), which has a pump-beam walk-off that is a factor of ~8 less than that of BBO; by replacing BBO with LBO in this design, a higher efficiency and improved beam symmetry are obtained in the region of enhanced stability; (5) the output from this single-stage system with spatiotemporal noise included in the model is described; the spatiotemporal evolution of the signal near the gain peak requires that a delicate balance be maintained between gain saturation and reconversion and that a trade-off must often be made between high output energy stability and low output beam intensity modulation.

Two-Stage Considerations discusses additional design considerations when a power amplifier is introduced. The amount of reconversion required in the preamplifier to achieve efficient and stable OPCPA output is generally greater when a power-amplification stage is added. Furthermore, proper matching of the seed- and pump-beam sizes in both the preamplifier and power amplifier maximizes the energy extracted from the pump. An optimized, two-stage OPCPA design for the front end of the OMEGA EP (extended performance) laser is presented. OMEGA EP is a petawatt-class, Nd-doped phosphate glass laser system that will be constructed at LLE to provide short-pulse backlighting capabilities, to investigate fast-ignition concepts for direct-drive inertial confinement fusion, and to study high-energy-density physics. The OMEGA EP front end must provide 5-Hz pulses with a minimum energy of 250 mJ and approximately 8-nm FWHM bandwidth centered at 1054 nm for injection into the main laser chain. The two-stage OPCPA design presented here provides over 500 mJ in a 1054-nm, 2.4-ns chirped pulse with nearly 8-nm FWHM bandwidth and 40% conversion efficiency using a 527-nm pump laser wavelength.

OPCPA Design Goals

In addition to gain variations caused by nonuniform intensity at the spatial and temporal edges of the pump, spatiotemporal intensity fluctuations produce localized variations in gain, causing nonuniform energy transfer from the pump to the signal. This can further reduce conversion efficiency and produce unwanted signal-beam modulation. Spatiotemporal modulation will also produce spatial and temporal variations in the onset of reconversion in the optical parametric amplification process, affecting the signal output energy stability.[15,16] Spatial walk-off of the pump from the signal beam can further reshape the latter. All of these issues are carefully addressed in attempting to achieve the following design goals for this OPCPA system:

1. *Maximize* pump energy extraction in each stage in order to reduce the pump average power requirement.
2. *Maintain* output signal energy stability at least as good as the pump input stability.
3. *Minimize* near-field modulation to reduce the risk of laser-induced damage to the front-end optics.
4. *Minimize* beam distortion caused by birefringent walk-off.

The current requirement for OMEGA EP is to produce compressed pulse widths of 1 to 100 ps. In the numerical model, the seed-pulse characteristics provided by a commercial mode-locked, Nd:glass laser system (GLX-200)[17] with a pulse width of 200 fs[7] were used. Since the stretched pulse width is in the nanosecond regime, the effects of the group-velocity mismatch between the pump, signal, and idler pulses are small and can be neglected in the analysis. Group-velocity dispersion is also negligible. As will be shown, spatial effects such as beam shape, pump–signal walk-off, beam-size matching, and intensity modulation significantly affect the ability to achieve the design goals.

Numerical Model

The coupled-wave equations for difference frequency generation in the slowly varying envelope approximation[18] were used in the numerical integration method following the form of Craxton[19] and taking into account the full spatial and temporal dependence of the three parametric waves,

$$\frac{\partial \tilde{E}_s(x,y,z,t)}{\partial z} = -\frac{1}{2}\gamma_s \tilde{E}_s(x,y,z,t) + \rho_s \frac{\partial \tilde{E}_s(x,y,z,t)}{\partial y}$$

$$-iK\tilde{E}_p(x,y,z,t)\tilde{E}_i^*(x,y,z,t)\exp(-i\Delta k\cdot z),$$

$$\frac{\partial \tilde{E}_i(x,y,z,t)}{\partial z} = -\frac{1}{2}\gamma_i \tilde{E}_i(x,y,z,t) + \rho_i(t)\frac{\partial \tilde{E}_i(x,y,z,t)}{\partial y}$$

$$-i\frac{\omega_2}{\omega_1}K\tilde{E}_p(x,y,z,t)\tilde{E}_s^*(x,y,z,t)\exp(-i\Delta k\cdot z), \quad (1)$$

$$\frac{\partial \tilde{E}_p(x,y,z,t)}{\partial z} = -\frac{1}{2}\gamma_p \tilde{E}_p(x,y,z,t) + \rho_p \frac{\partial \tilde{E}_p(x,y,z,t)}{\partial y}$$

$$-i\frac{\omega_3}{\omega_1}K\tilde{E}_s(x,y,z,t)\tilde{E}_i(x,y,z,t)\exp(i\Delta k\cdot z),$$

where subscripts s, i, and p refer to the signal, idler, and pump waves, respectively; γ is the absorption coefficient; ω is the angular frequency of the electric field; and t is the reduced time taken in the reference frame of the pulse. $\tilde{E}$ is the complex field amplitude that has been scaled by $n^{1/2}$, where n is the refractive index of the wave derived from a Sellmeier equation.[20] The energy flux for each wave is thus proportional to $|\tilde{E}|^2$. The birefringence walk-off angle of the pump is given by ρ_p, whereas ρ_s and ρ_i account for the possibility of a noncollinearity among the wave vectors. By energy conservation, $\omega_i = \omega_p - \omega_s$ and the wave-vector mismatch is $\Delta k = k_p - k_i - k_s$. For a noncollinear angle ρ_s between the signal- and pump-wave-vector directions, Δk and the direction ρ_i of the idler-wave vector in the crystal are determined from the cosine rule.[12] Note that the temporal chirp of the signal pulse gives a spread in idler propagation directions. K is defined as

$$K = \frac{\omega_1}{c}\left(n_s n_i n_p\right)^{-1/2} d_{\text{eff}}, \quad (2)$$

where d_{eff} is the effective nonlinear coefficient for the type-I parametric interaction.

A split-step technique was used where Eqs. (1) were solved in the space-time domain, and spatial walk-off and noncollinear propagation were performed in the spatial-frequency domain. A linear chirp with 8-nm FWHM bandwidth was superimposed upon a 1054-nm Gaussian temporal and spatial seed for input to the optical parametric amplifier (OPA) crystals, and a 527-nm single-frequency pump was used with type-I phase matching in both collinear and noncollinear geometries. Both simulated and experimentally measured spatial and temporal shapes can be used as input to the model, and the output is available in both spatially and temporally resolved and integrated forms. Experimentally measured inputs were used in the model to achieve excellent agreement with previous experimental results[7] and were used in the current analysis to investigate the effect of pump-beam spatiotemporal noise on the OPCPA output. In order to perform a systematic investigation of how specific design parameters affect OPCPA output, simulated beam shapes without spatiotemporal noise were also used.

Single-Stage Design Considerations

The OPCPA designs presented in this section consist of two crystals configured as a single stage with no idler separation between the crystals. The air gap between the two crystals is assumed to be zero in the model since a gap of less than ~4 mm introduces negligible dephasing in the conversion process.[7] These designs provide nominally 5-mJ output energy using a pump intensity of 1 GW/cm^2 and a FWHM pulse width and nominal beam diameter of 1 ns and 1.5 mm, respectively (pump energy ≈ 18 mJ). The pump has a tenth-order super-Gaussian temporal and spatial shape, and the seed is Gaussian in time and space with FWHM of 1 ns and 1.5 mm, respectively. The seed input energy is 800 pJ. The considerations discussed here are also applicable for the energy-scaled designs appropriate for the OMEGA EP front end, discussed in **Two-Stage Considerations**.

Figure 95.20 shows the output signal energy versus the length of the second crystal for two different single-stage preamplifier designs, one using two BBO crystals and the other two LBO crystals. The first-crystal lengths are 10 mm and 25 mm for the BBO and LBO designs, respectively. The solid curves in Fig. 95.20 represent the nominal pump intensity of 1 GW/cm^2; the dashed curves represent pump intensities that

are ±5% about this nominal value. These design parameters were chosen based on the measured damage threshold of the antireflective coatings on the OPA crystals. The region of highest stability for each design in Fig. 95.20 is just past the peak of the gain curve where reconversion begins.[15] The detailed performance of the BBO design without spatiotemporal noise on the pump beam along with the LBO design are discussed in the next two subsections. Higher efficiency and better beam shape are achieved for LBO in the region of enhanced stability, and a trade-off must be made among efficiency, stability, and near-field beam modulation. For the LBO design, we show that this trade-off exists both with and without the inclusion of spatiotemporal noise on the pump beam.

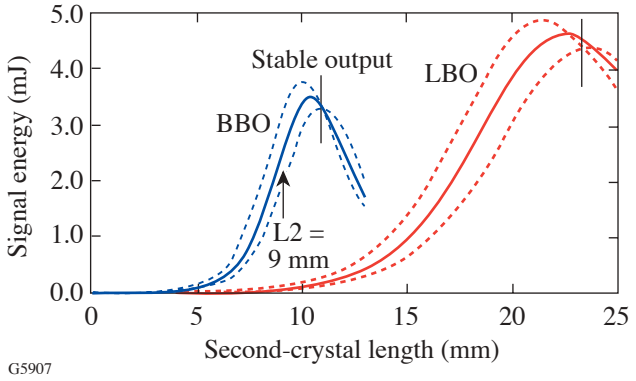

Figure 95.20
Signal output energy versus length of the second crystal for two-crystal, single-stage BBO and LBO preamplifier designs. The solid curves represent the nominal pump input intensity of 1 GW/cm^2, and the dashed curves represent ±5% about this intensity. The crystal lengths that provide enhanced stability for each design are indicated by the vertical lines on the graph. The input pump and seed spatial and temporal shapes are the same for both designs, except that the pump beam is narrower in the direction orthogonal to walk-off by 9% for the LBO design and 20% for the BBO design. The arrow indicates the second-crystal length of 9 mm for the BBO design shown in Fig. 95.21(a) and discussed in the text.

1. BBO Preamplifier

The BBO preamplifier consists of two BBO crystals configured for type-I phase matching whose extraordinary axes are oriented in opposing directions for walk-off compensation.[21] To achieve large pump-energy extraction using flattop shapes, the pump and signal widths must be well matched in the second crystal where most of the pump-energy extraction occurs. The pump–signal walk-off causes spatial gain narrowing to be greater in the walk-off direction, leading to output beam ellipticity and reduced conversion efficiency. Proper walk-off compensation requires a combination of opposing crystal orientations, lateral displacement of the seed and pump beams on the first crystal's face, and anamorphic pump beam shaping.[6,21] Figure 95.21(a) shows the output signal-beam shape obtained just before the peak of the BBO gain curve in Fig. 95.20 for first- and second-crystal lengths of L1 = 10 mm and L2 = 9 mm, respectively, and a collinear phase-matching condition. The pump-beam FWHM used in Fig. 95.21 was 1.5 mm in the walk-off direction, but 20% smaller in the direction orthogonal to walk-off. The pump-beam center was offset from the seed-beam center on the first crystal's face by 280 μm opposite to the pump-beam walk-off direction (upward in Fig. 95.21). For a second-crystal length of 9 mm, the predicted efficiency of 16.9% is quite good, and the output beam shape shows little asymmetry in the walk-off direction; however, the stability is poor [see Fig. 95.20 and Fig. 95.21(a)].

Better efficiency and improved stability are obtained at the peak of the gain curve; however, spatial variations in saturation and reconversion produce intensity modulation and beam asymmetry in the walk-off direction, as shown in Fig. 95.21(b). The region of best stability is with a second-crystal length of 10.9 mm (see Fig. 95.20), but the beam shape is further degraded with a peak-to-valley modulation of ~30%, as shown in Fig. 95.21(c). A noncollinear phase-matching angle may be considered in order to reduce the pump–signal walk-off within the crystals; however, a limitation exists because the idler beam will walk out of the interaction area even if the pump- and signal-beam propagation directions within the crystals are perfectly collinear. This effect is significant in BBO because of its large walk-off angle (~3.2°). In addition, the maximum bandwidth in a degenerate OPA is achieved in a nearly collinear geometry.[2] Typically, an external angle of ~0.5° in air between the pump and seed beams is used to separate the signal and idler outputs. Figure 95.21(d) shows the output signal-beam shape for an external noncollinear beam angle of 0.5° and crystal lengths that provide enhanced stability. In this case the seed beam is tilted in the direction of pump-beam walk-off in the first crystal, and only a small difference is seen between the collinear and slightly noncollinear configurations [compare Figs. 95.21(c) and 95.21(d)]. Figure 95.22 shows that gain narrowing of the chirped signal pulse is greater for the shorter crystal length, but slight pulse broadening is observed when saturation is large.

2. LBO Preamplifier

The sensitivity of beam shape to beam angle and interaction length in BBO can be alleviated to a large extent through the use of LBO. LBO has a pump walk-off angle that is a factor of ~8 smaller than that in BBO, a larger angular acceptance, and a sufficiently high nonlinear coefficient to make it preferable

to BBO for this application.[20] Although LBO has a larger refractive-index variation with temperature than BBO, the measured output stability at a 5-Hz repetition rate is better than that of the pump when the crystals are held in a temperature-controlled oven at 32°C (Ref. 7). Figure 95.20 shows the signal output energy of an LBO design that uses nearly identical input beam parameters as the BBO design. As with the BBO design, the pump-beam FWHM is matched to the seed-beam FWHM in the walk-off direction, but because the pump walk-off angle is less in LBO, the pump input beam FWHM in the direction orthogonal to walk-off is smaller by only 9% compared with 20% for BBO. This allows more pump energy to be used while maintaining the same average pump intensity of 1 GW/cm^2. The output signal energy at peak conversion is thus greater. The smaller walk-off angle allows greater efficiency at the second-crystal length L2 = 23.5 mm, where stability is highest (η = 27.7% for LBO versus η = 24.2% for BBO). The effect of ±5% seed fluctuations on the output stability is much less than 1% for the level of seed energy used (800 pJ). Additional simulations have shown that the conversion efficiency for this LBO design can approach 40% if 30th-order super-Gaussian pump shapes are used with standard Gaussian seed shapes.

Figure 95.23(a) shows the simulated output beam shape for the LBO design in the region of greatest stability. This design provides less azimuthal beam variation and higher efficiency than the BBO design [compare Figs. 95.21(d) and 95.23(a)]. The pump-beam walk-off angle in LBO is close to the 0.5° noncollinear angle between the pump and seed input beams typically used to allow separation of the idler and signal

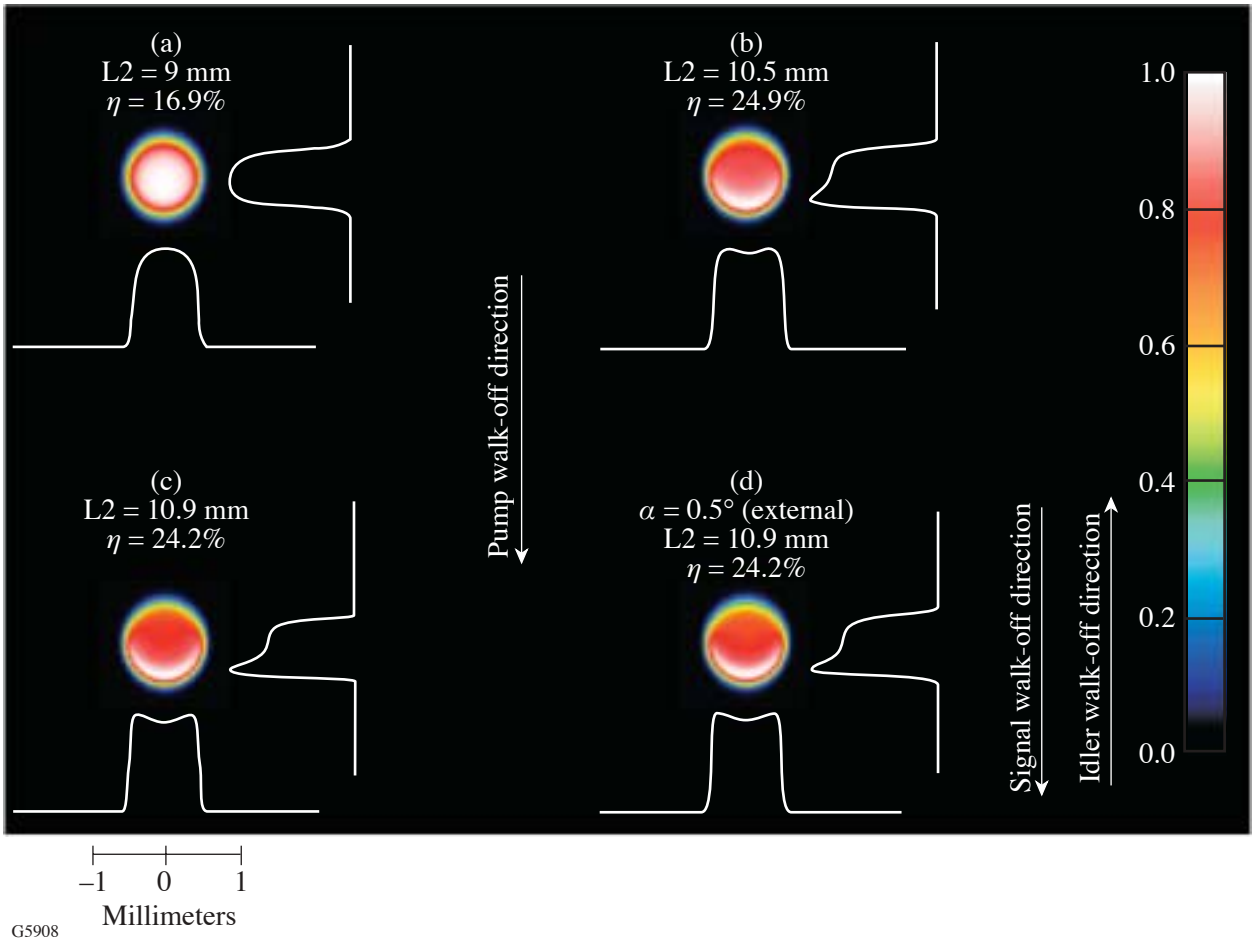

Figure 95.21
Temporally integrated, normalized signal output beam shapes for the single-stage BBO design with different second-crystal lengths L2 for L1 = 10 mm. Stability for each case is shown in Fig. 95.20. (a) L2 = 9 mm (undersaturated), (b) L2 = 10.5 mm (peak of the gain curve), (c) L2 = 10.9 mm (region of enhanced stability), and (d) L2 = 10.9 mm with an external noncollinear angle of 0.5° between the pump and seed beams. Conversion efficiencies η are indicated in the figure.

outputs; thus, for this LBO design, both crystals are oriented identically and a noncollinear angle of 0.5° is used with the pump beam offset from the seed beam by 187 μm on the first crystal's face [vertically upward in Fig. 95.23(a)]. Figure 95.23(b) shows the temporal output for the design of Fig. 95.23(a). The greater reconversion seen in the spatial and temporal center of the signal output beam in Fig. 95.23 is a result of the Gaussian spatial and temporal shape of the seed beam. Less reconversion is seen in the spatially integrated temporal profile shown in Fig. 95.23(b). In addition to the better overall performance achieved with LBO, this design approach shows that BBO can be retrofitted with LBO, if desired, with only a change in pump-beam energy and ellipticity (by use of a prism, for example). An overall change in beam size is not required. Alternatively, using LBO instead of BBO has the advantage that a smaller aperture size is required to extract the same amount of pump energy, potentially reducing optical component cost.

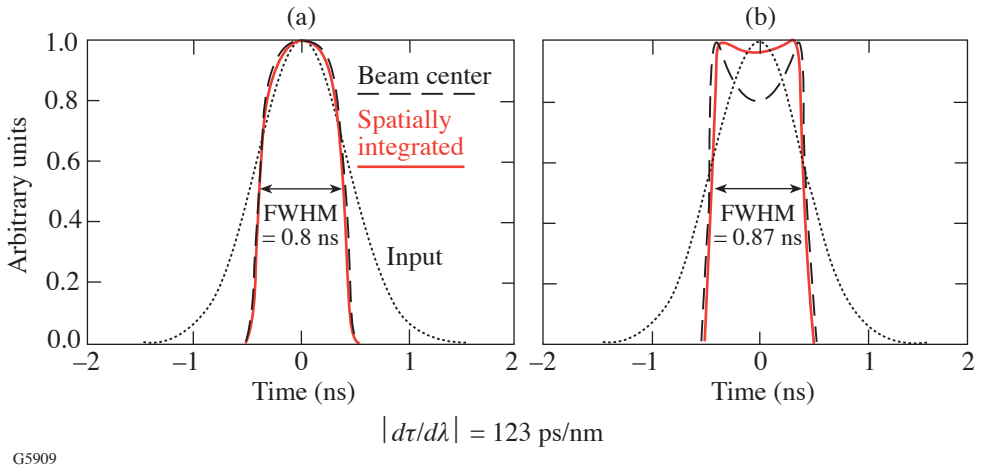

Figure 95.22
Normalized, temporal profiles for two of the BBO designs shown in Fig. 95.21. The simulation uses a 200-fs Gaussian temporal pulse that is stretched in time to provide a linearly chirped, 1.0-ns input seed pulse to the crystals. Beam center: dashed; spatially integrated: solid; input: dotted. (a) For the case of Fig. 95.21(a), the pulse shape shows little saturation and a gain-narrowing effect. (b) Saturation with reconversion is seen for the case of Fig. 95.21(d), contributing to a broadening of the pulse compared with Fig. 95.22(a). Greater reconversion is seen at beam center because of the spatial Gaussian shape of the seed.

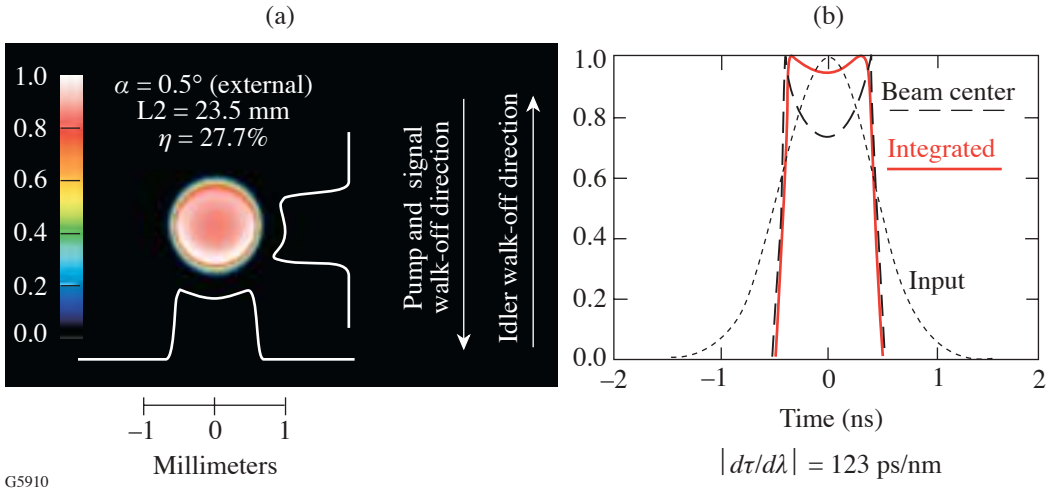

Figure 95.23
(a) Temporally integrated, normalized signal output beam shape for the single-stage LBO design in the region of enhanced stability (L2 = 23.5 mm in Fig. 95.20). The ~15% dip in the center is from greater reconversion in this region as a result of the Gaussian shape of the seed beam. (b) Normalized temporal profile of input seed and output signal pulses for the case shown in Fig. 95.23(a).

3. LBO Design with Spatiotemporal Noise

The experimentally measured[7] pump spatial and temporal shapes used in the LBO design are shown in Fig. 95.24 to illustrate how pump-beam intensity modulation affects the signal output near the peak of the gain curve. In this simulation, each temporal slice of the pump beam shown in Fig. 95.24(a) is assigned a flat phase front and the same normalized spatial modulation (peak-to-mean = 25% within an area defined by 60% of the pump beam's spatial FWHM). The pump temporal pulse shape is shown in Fig. 95.24(b) and has a modulation of ~10%. Figures 95.24(c) and 95.24(d) show two temporal slices of the output signal beam, one at the peak and one at the dip of the pump pulse. The signal-beam temporal slices, separated in time by 210 ps, clearly show a spatiotemporal coupling and a delicate balance between gain saturation and reconversion. Localized regions in the signal beam corresponding to high peak intensity in the pump beam are just beginning to reconvert at the dip of the pulse and are farther into reconversion at the peak of the pulse. In both cases, the output beam has lower peak-to-mean modulation than the pump beam. Greater smoothing is observed at the peak of the pulse due to greater overall saturation. Figure 95.25 plots the normalized output energy and temporally integrated output beam modulation for this design versus the normalized pump-beam input energy, showing that a trade-off exists in this case between intensity modulation and output energy stability. For the pump energy that provides both maximum output energy and maximum output energy stability (dotted vertical line in Fig. 95.25), the output beam modulation is less than that of the pump beam. At the peak of the output energy curve, the output energy changes by ±2% for pump energy fluctuations of ±5%.

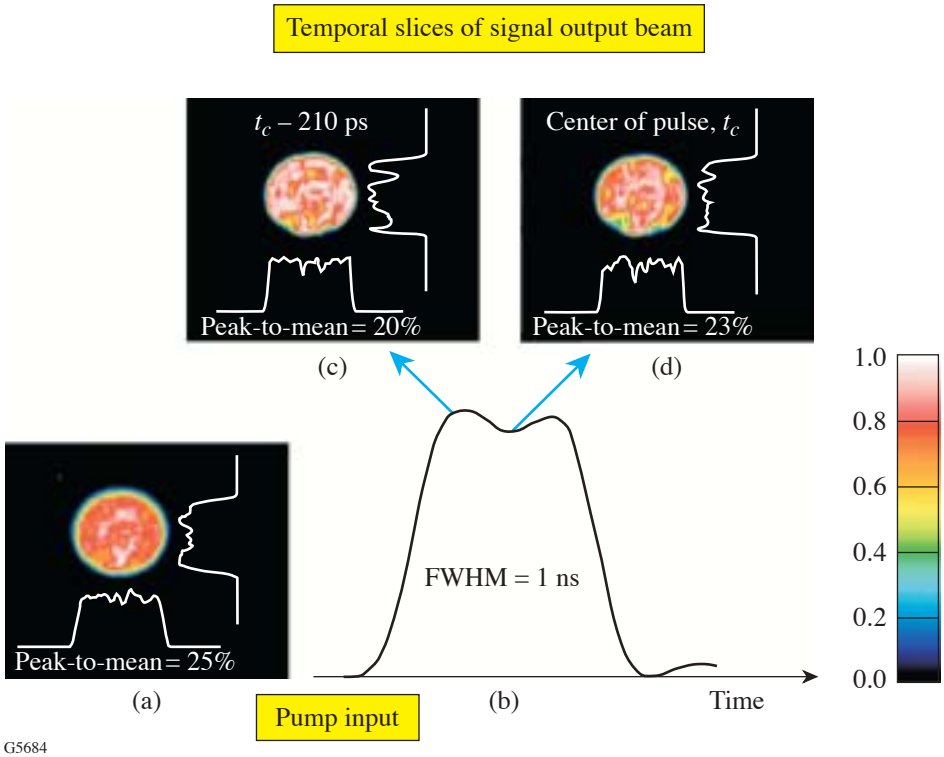

Figure 95.24
Experimentally measured pump (a) spatial and (b) temporal shapes are used to illustrate how pump-beam intensity modulation affects the signal output near the peak of the gain curve. Two temporal slices of a simulation of the output signal beam are shown in (c) and (d); one at the peak and one at the dip of the pump pulse, respectively.

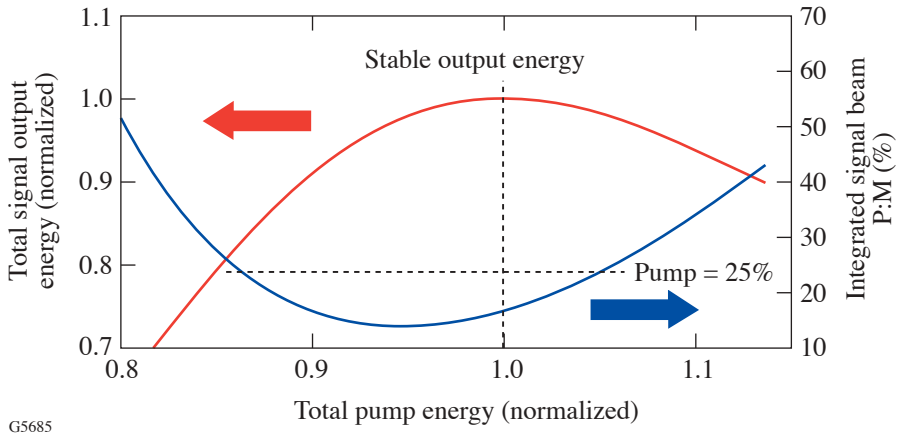

Figure 95.25
Comparison of the output energy and output beam quality for a single-stage LBO design. The axis on the left indicates the normalized signal output energy versus normalized pump input energy, while the axis on the right gives the output signal beam's peak-to-mean intensity modulation. The graphs show that a trade-off exists between enhanced energy stability and low near-field intensity modulation.

Two-Stage Considerations

1. Preamplifier Modification

As noted in the previous section, the OMEGA EP front-end energy requirement of 250 mJ for injection into the Nd:glass amplifier chain requires both an energy-scaled preamplifier design and a power amplifier. Square beams will be used to provide a better fill factor than round beams in the OPA crystals and the Nd:glass multipass disk amplifiers, improving the energy extraction. A block diagram with nominal pump and signal energies for the prototype OMEGA EP OPCPA front end is shown in Fig. 95.26. The design consists of two LBO crystals configured as a single preamplifier stage followed by an LBO power amplifier. Details of this design are given in the next subsection. The design guidelines discussed for a high-efficiency, single-stage OPCPA system are similar to those required when the power amplifier is introduced.

Figures 95.27(a)–95.27(c) are simulated plots of the signal output energy from a two-stage, all-LBO design versus the length of the power amplifier for three different preamplifier lengths. The pump input beam used in these simulations was square and had a simulated, Gaussian, randomly distributed intensity modulation of 25% peak-to-mean so that the two-stage OPCPA system could be optimized simultaneously for efficiency, stability, and beam quality.

For the undersaturated preamplifier in Fig. 95.27(a), a power-amplifier length of ~14 mm provides high output stability but relatively low output energy. A preamplifier operated with a small amount of reconversion is stable, as shown in Fig. 95.27(b), but does not provide sufficient stability in the power amplifier. Increasing the preamplifier length causes the power-amplifier stable region [at the foot of the three curves in

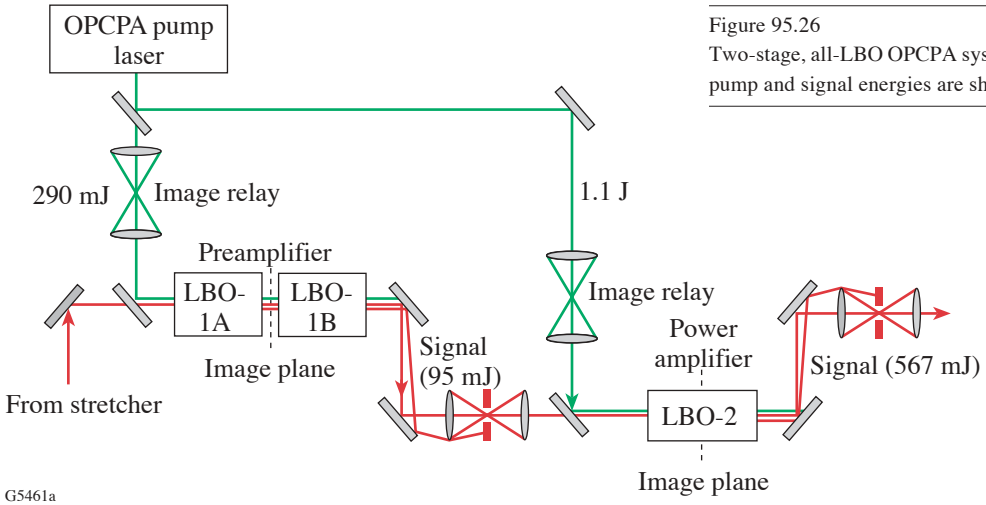

Figure 95.26
Two-stage, all-LBO OPCPA system for the OMEGA EP front end. Nominal pump and signal energies are shown.

Fig. 95.27(b)] to move up the curve to a region of higher efficiency. Figure 95.27(c) shows that extending the preamplifier length by 2 mm provides high output energy and enhanced stability in the power amplifier. As noted for a single-stage OPCPA system, a trade-off between stability, efficiency, and beam quality also exists for a two-stage system. Care must be exercised when extending the length of the preamplifier since more reconversion may increase the preamplifier output spatiotemporal modulation beyond that of the pump beam, possibly putting downstream optics at risk. For the design of Fig. 95.27(c), the peak fluence at the output of the preamplifier is less than or equal to that of the pump.

2. "Mode-Matching" and OMEGA EP OPCPA Design

Maximizing the conversion efficiency in the power amplifier also requires that the power-amplifier seed- and pump-beam sizes be properly matched. By allowing the power-amplifier seed-beam size to closely match the pump-beam size, energy at the edges of the pump beam can be efficiently extracted. Little spatial gain narrowing is seen in the power amplifier because of the steep edges of both the seed and pump beams and because the gain is no longer exponential.

The prototype OPCPA front end for OMEGA EP (Fig. 95.26) was designed for the amplification of a temporally stretched, 2.4-ns, 1054-nm seed pulse. The preamplifier consists of two 5 × 5 × 29.75-mm crystals configured as a single stage with no idler separation between the crystals. The power amplifier is 10 × 10 × 11 mm. The crystals are cut at 11.8° in the *x*-*y* plane of the crystal for type-I angular phase matching at 32°C. At a pump intensity of 1 GW/cm^2, the expected conversion efficiency is 40% with over-500-mJ signal output energy, a gain of greater than 5 × 10^9, and an output energy stability about equal to that of the pump.

Figure 95.28 shows how overall conversion efficiency, output energy, and output stability scale with the relative size of the seed and pump beams. The pump temporal and spatial super-Gaussian orders used in this design are 10 and 20, respectively, and the seed is Gaussian in space and time.

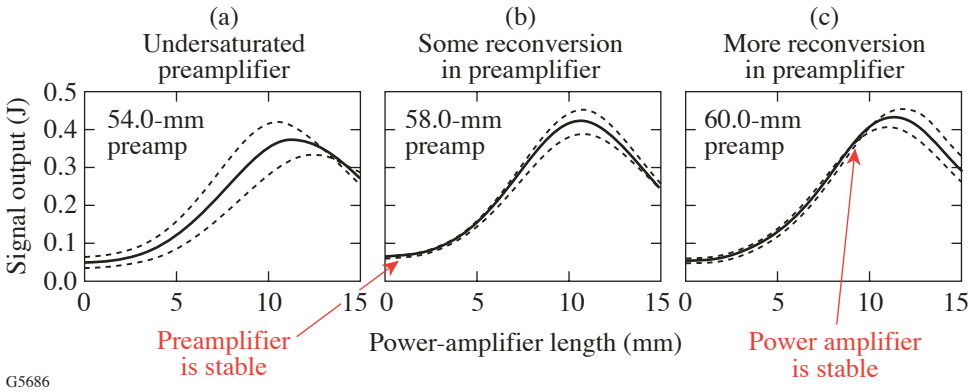

Figure 95.27
Simulated plots of the signal output energy from the two-stage, all-LBO design shown in Fig. 95.26 versus the length of the power amplifier for three different preamplifier lengths. Solid lines represent the nominal pump input intensity of 1 GW/cm^2, whereas the dashed lines represent ±5% about this nominal intensity.

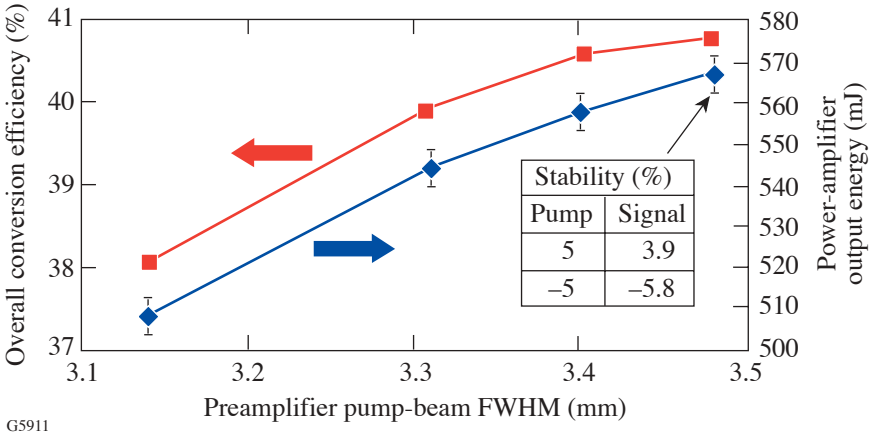

Figure 95.28
Plot of conversion efficiency (squares) and output energy (diamonds) for a two-stage OPCPA design versus the preamplifier input pump beam's size. The pump input beam is a 20th-order super-Gaussian with nominal intensity of 1 GW/cm^2 for each point plotted. The seed beam of the preamplifier is Gaussian with FWHM of 3.18 mm. The error bars indicate output energy changes for ±5% pump energy fluctuations.

For the two-stage design of Fig. 95.28, the input pump beam's size and intensity at the power amplifier are kept fixed, while the input pump beam's size at the preamplifier is varied with its intensity held constant by scaling its energy. The size of the seed beam at the preamplifier and the signal-beam magnification between the two stages are kept fixed; thus the average signal intensity in both stages does not change significantly as the input pump beam's size in the preamplifier is varied. Maintaining approximately constant input intensity of the signal and pump beams in both stages allows the enhanced stability condition to be maintained and, at the same time, allows the relative size of the seed and pump beams to be varied.

Because the seed beam at the input to the preamplifier is Gaussian, the variation of the pump beam's size at the input of the preamplifier produces an effective change in the preamplifier output signal beam size, and thus, the size of the signal beam at the input to the power amplifier. Figure 95.29 shows how the signal beam's size entering the power amplifier changes with the size of the preamplifier pump beam. From Figs. 95.28 and 95.29, it is seen that output stability is essentially unchanged when the preamplifier pump beam's size is varied, while seeding the power amplifier with a beam that is smaller than the pump-beam FWHM of 6.8 mm degrades the efficiency. Closely matching the pump and signal beams' sizes at the input to the power amplifier ensures highly efficient extraction of the pump-beam energy at its edges.

The output spatial-intensity distribution for this two-stage design with simulated, Gaussian, randomly distributed spatiotemporal noise on the pump beam is shown in Fig. 95.30. The output pulse shape and phase accumulated in the OPA are shown in Fig. 95.31. The quadratic temporal phase is due to the phase mismatch across the chirped input seed pulse. Heavy saturation in the power amplifier produces an output signal beam with less spatiotemporal noise than the input pump beam.

Conclusion

We have described the detailed spatiotemporal behavior of the OPCPA process using a combination of Gaussian and super-Gaussian spatial and temporal shapes and have included the effects of pump spatiotemporal noise and pump–signal spatial walk-off. Using a three-dimensional spatial and temporal numerical model, we have shown that for single-stage OPCPA systems that operate in both the small-signal (i.e., high gain) and high-saturation regimes, the spatial and temporal gain–narrowing effect can be reduced with high-order super-Gaussian pump shapes, leading to high conversion efficiency, as demonstrated in our earlier experimental work.[7] Additional simulations have shown that the conversion efficiency for a slightly non-degenerate, type-I parametric process can approach 40% using 30th-order super-Gaussian pump shapes in a single-stage OPCPA system with standard Gaussian seed shapes.

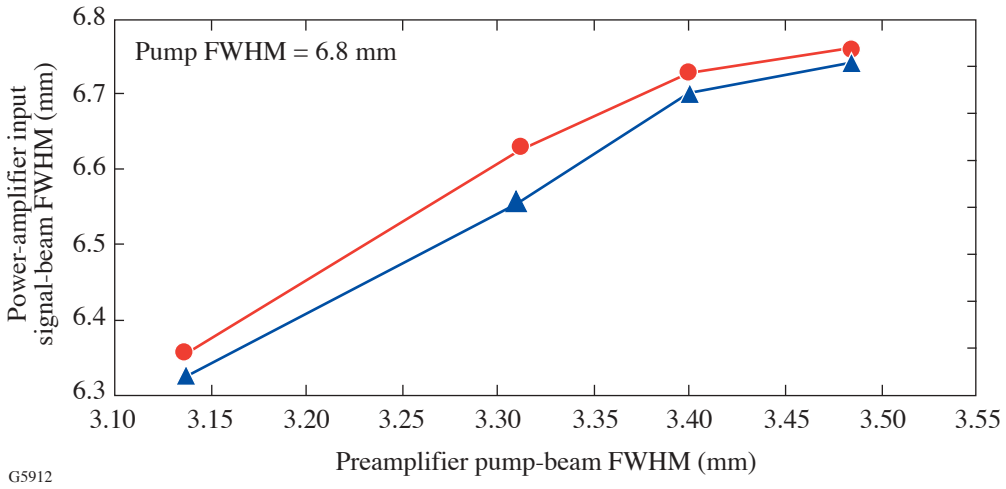

Figure 95.29
Size of the signal beam entering the power amplifier versus preamplifier pump beam's size for the two-stage design of Fig. 95.28. Triangles: in the direction of pump-beam walkoff; circles: orthogonal to walk-off. The FWHM of the pump beam entering the power amplifier is 6.8 mm.

We have also shown that the large pump–signal walk-off in BBO makes it difficult to simultaneously achieve high conversion efficiency, stable output, and good beam quality in this material. An LBO design using nearly identical input beam parameters has been shown to provide better beam quality and conversion efficiency at the crystal length where output stability is highest. A tradeoff among the efficiency, stability, and beam quality both with and without pump spatiotemporal noise has been shown, emphasizing the importance of modeling the full spatial and temporal dependence for design optimization. For the optimized LBO design, both output energy fluctuations and spatiotemporal intensity modulations were less than those of the pump.

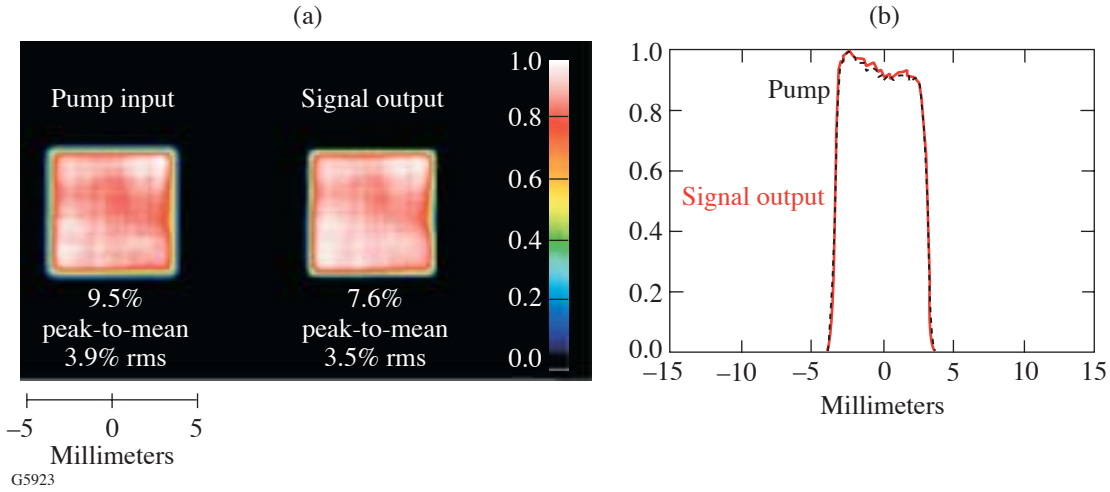

Figure 95.30
For the design shown in Figs. 95.28 and 95.29 with preamplifier pump beam's FWHM = 3.48 mm: (a) Normalized beam cross section for the temporally integrated pump-beam input with simulated, spatiotemporal noise (left) and the power-amplifier signal output beam (right); (b) normalized horizontal lineouts through the center of each of the beams shown in (a). Signal: solid; pump: dashed.

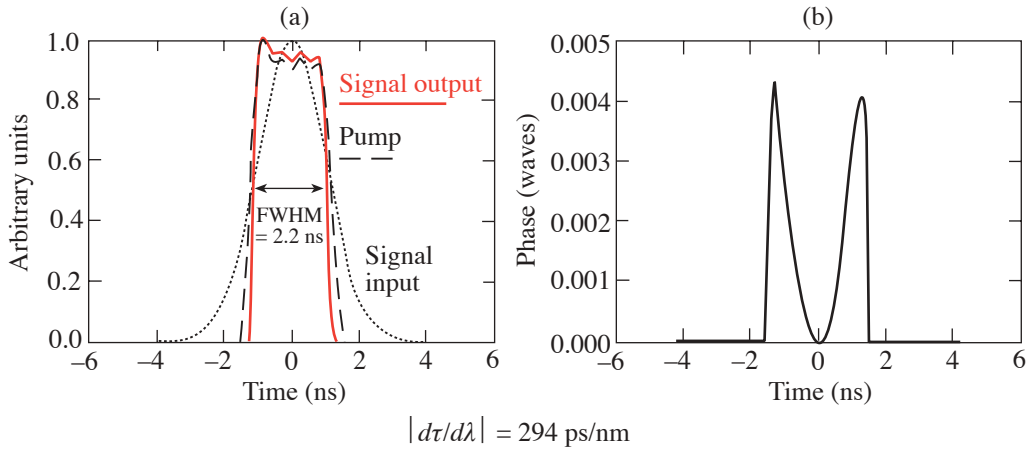

Figure 95.31
(a) Spatially integrated, normalized temporal profiles of the input pump and signal input/output pulses for the two-stage design with preamplifier pump beam's FWHM = 3.48 mm. The seed pulse entering the first crystal of the preamplifier is shown dotted; the signal pulse out of the power-amplifier crystal is shown solid. The pump input temporal noise is 11% peak-to-valley (3% rms), whereas the amplified signal output temporal noise is only 8% peak-to-valley (2% rms). The spectral bandwidth of the output pulse is 7.5 nm. (b) Phase accumulated in the OPA for the chirped output pulse shown in (a).

The design guidelines discussed for a single-stage preamplifier were applicable when a power amplifier was added, but it was found that the preamplifier had to be operated farther into reconversion in order to obtain high efficiency and stable output from the power amplifier. Adjusting the relative size of the pump and input signal beams at the power amplifier was necessary to maximize conversion. By closely matching the pump and signal beams' sizes at the input to the power amplifier, better extraction of the pump-beam energy at its edges is achieved. These guidelines were used to design the prototype OMEGA EP OPCPA front end that met each of the design goals discussed in **OPCPA Design Goals**. This design should provide nearly 40% conversion efficiency, with stability and beam quality at least as good as that of the pump.

ACKNOWLEDGMENT

This work was supported by the U.S. Department of Energy Office of Inertial Confinement Fusion under Cooperative Agreement No. DE-FC03-92SF19460, the University of Rochester, and the New York State Energy Research and Development Authority. The support of DOE does not constitute an endorsement by DOE of the views expressed in this article.

REFERENCES

1. A. Dubietis, G. Jonusauskas, and A. Piskarskas, Opt. Commun. **88**, 437 (1992).
2. I. N. Ross *et al.*, Opt. Commun. **144**, 125 (1997).
3. I. N. Ross *et al.*, Appl. Opt. **39**, 2422 (2000).
4. H. Yoshida *et al.*, in *Conference on Lasers and Electro Optics*, Vol. 1, Technical Digest (Optical Society of America, Washington, DC, 2001), pp. 80–81.
5. X. Yang *et al.*, Opt. Lett. **27**, 1135 (2002).
6. I. Jovanovic *et al.*, Appl. Opt. **41**, 2923 (2002).
7. L. J. Waxer, V. Bagnoud, I. A. Begishev, M. J. Guardalben, J. Puth, and J. D. Zuegel, "High-Conversion-Efficiency, Optical Parametric Chirped-Pulse-Amplification System Using Spatiotemporally Shaped Pulses," submitted to Optics Letters.
8. I. A. Begishev, A. A. Gulamov, E. A. Erofeev, E. A. Ibragimov, S. R. Kamalov, T. Usmanov, and A. D. Khadzhaev, Sov. J. Quantum Electron. **20**, 1100 (1990).
9. I. A. Begishev, A. A. Gulamov, E. A. Erofeev, E. A. Ibragimov, S. R. Kamalov, T. Usmanov, and A. D. Khadzhaev, Sov. J. Quantum Electron. **20**, 1104 (1990).
10. L. J. Waxer, J. H. Kelly, J. Rothenberg, A. Babushkin, C. Bibeau, A. Bayramian, and S. Payne, Opt. Lett. **27**, 1427 (2002).
11. M. D. Skeldon, Rev. Sci. Instrum. **71**, 3559 (2000).
12. I. N. Ross *et al.*, J. Opt. Soc. Am. B **19**, 2945 (2002).
13. M. D. Perry, F. G. Patterson, and J. Weston, Opt. Lett. **15**, 381 (1990).
14. Z. Pengfei *et al.*, Opt. Laser Technol. **35**, 13 (2003).
15. S. K. Zhang *et al.*, Opt. Commun. **184**, 451 (2000).
16. M. J. Guardalben, J. Keegan, L. J. Waxer, and J. D. Zuegel, presented at the 2002 OSA Annual Meeting, Orlando, FL, 29 September–3 October 2002.
17. Time-Bandwidth Products, Inc., Zürich, Switzerland, CH-8005 (http://www.tbwp.com).
18. J. A. Armstrong *et al.*, Phys. Rev. **127**, 1918 (1962).
19. R. S. Craxton, IEEE J. Quantum Electron. **QE-17**, 1771 (1981).
20. V. G. Dmitriev, G. G. Gurzadyan, and D. N. Nikogosyan, *Handbook of Nonlinear Optical Crystals* (Springer-Verlag, Berlin, 1991), p. 78.
21. D. J. Armstrong *et al.*, J. Opt. Soc. Am. B **14**, 460 (1997).